# Gas Sensing with Au-Decorated Carbon Nanotubes

**Zeila Zanolli,[†,⊥,*] Radouane Leghrib,[‡] Alexandre Felten,[§] Jean-Jacques Pireaux,[§] Eduard Llobet,[‡] and Jean-Christophe Charlier[†]**

[†]Institute of Condensed Matter and Nanosciences (IMCN), Université Catholique de Louvain, Place Croix du Sud 1 (NAPS-ETSF-Boltzmann), 1348 Louvain-la-Neuve, Belgium, [‡]MINOS-EMaS, Universitat Rovira i Virgili, Avenida Paisos Catalans, 26, 43007 Tarragona, Spain, and [§]Research Centre in Physics of Matter and Radiation (PMR), Facultés Universitaires Notre-Dame de la Paix, Rue de Bruxelles 61, B-5000 Namur, Belgium. [⊥]Present address: Physics Department, University of Liege, B-4000 Sart Tilman, Liege, Belgium

**ABSTRACT** The sensing properties of carbon nanotubes (CNTs) decorated with gold nanoparticles have been investigated by means of combined theoretical and experimental approaches. On one hand, first-principles and nonequilibrium Green's functions techniques give access to the microscopic features of the sensing mechanisms in individual nanotubes, such as electronic charge transfers and quantum conductances. On the other hand, drop coating deposition of carbon nanotubes decorated with gold nanoparticles onto sensor substrates and their characterization in the detection of pollutants such as $NO_2$, CO, and $C_6H_6$ provide insight into the sensing ability of nanotube mats. Using the present combined approaches, the improvement in the detection of some specific gases ($NO_2$ and CO) using Au-functionalized nanotubes is explained. However, for other gases such as $C_6H_6$, the Au nanoparticles do not seem to play a crucial role in the sensing process when compared with pristine CNTs functionalized with oxygen plasma. Indeed, these different situations can be explained by identifying the relationship between the change of resistance (macroscopic feature) and the shift of the Fermi level (microscopic feature) after gas adsorption. The understanding of the sensing ability at the atomic level opens the way to design new gas sensors and to tune their selectivity by predicting the nature of the metal that is the most appropriate to detect specific molecular species.

**KEYWORDS:** carbon nanotubes · room temperature gas sensing · metal nanoparticle decoration · electronic structure · quantum transport · oxygen plasma treatment

Carbon nanotubes (CNTs)[1] are attractive materials both as benchmarks of fundamental physical properties in a one-dimensional nanosystem[2,3] and for a wide variety of nanotechnology applications, for instance, in electronics,[4] spintronics,[5−8] or biotechnologies.[9−11] In particular, due to their high surface to volume ratio and being characterized by a conductance that can be easily perturbed by interaction with gas molecules, CNTs are promising candidates as active elements for extremely sensitive gas-sensing devices.[12] However, the response of pristine CNTs to gases is weak and scarcely selective since the ideal carbon hexagonal network is held together by strong $sp^2$ bonds characterized by a low chemical reactivity with the molecular environment. Consequently, the functionalization of the CNT sidewalls is mandatory to improve both the sensitivity and the selectivity of CNT-based gas sensors.[13] In particular, functionalization with metal nanoparticles (NPs) can lead to highly sensitive and selective gas sensors thanks to the extraordinary catalytic properties of metal NPs,[14] as already suggested by several experimental,[15−22] theoretical,[23−25] and combined[26,27] works.

Although the sensing ability of CNTs decorated with metal NPs relies on the huge chemical reactivity of the cluster surface, the whole CNT-NP system acts as *the detection unit* of the device. Indeed, the interaction with gas molecules results in an electronic charge transfer between the molecule and the CNT-NP sensor, which affects the position of the Fermi energy and, hence, the conductivity of the detection unit. Such a conductivity modification can, for instance, be measured by embedding mats of metal-decorated multiwall carbon nanotubes (MWNTs) in a standard electronic device.[21,28] Since these mats usually behave as p-doped semiconductors, the adsorption of an extra electron coming from molecules exhibiting a donor character will induce an increase of the resistance. Analogously, the interaction with molecules exhibiting an acceptor character will lead to a decrease of the resistance. In addition, functionalization of CNTs with metal nanoparticles can be exploited to improve the sensor selectivity, since different metals will present different reactivities toward different molecules. Hence, a gas sensor device can be fabricated by depositing on a microsensor array several sets of MWNT mats, each decorated with different types of metallic NPs.[21]

## RESULTS AND DISCUSSION

In the present work, a combined theoretical and experimental investigation of the

* Address correspondence to zeilazanolli@gmail.com.

Received for review January 24, 2011 and accepted May 9, 2011.

**Published online May 09, 2011**
**10.1021/nn200294h**

sensing response of CNTs decorated with gold NPs is proposed in order to understand accurately the detection ability of these nanosystems to specific gas species. On one hand, electrical transport measurements provide information on the behavior of the CNT-NP detection unit at the macroscopic scale by measuring its resistance changes. On the other, first-principles modeling allows one to address the problem from a microscopic point of view, giving information on the electronic charge transfer, the interaction strength (such as binding energies and bond lengths), and the quantum electron conductance. The two approaches are complementary since they are both needed to achieve a complete description of the gas-sensing mechanisms from the macroscopic to the atomic scale. Gold nanoparticles are chosen as the sensing metal since the Au cluster interacts weakly with the carbon $sp^2$ network,[29] and hence, such a functionalization perturbs the electronic and transport properties of the host nanotube only slightly. In order to illustrate different sensing responses, molecules that cause a decrease ($NO_2$, acceptor character) or an increase ($C_6H_6$, donor character) or leave unaffected (CO) the Fermi energy of the Au-CNT system are considered. The present combined approaches explain why Au functionalization can improve the detection of some gases ($NO_2$, CO) but not of others ($C_6H_6$) and allow the identification of the correlation between the resistance changes after gas adsorption measured experimentally and the corresponding shift of the Fermi energy computed theoretically.

**Experiment.** The sensing properties of Au-MWNTs operated at room temperature are investigated by exposing them to different chemical environments ($NO_2$, CO, $C_6H_6$) and various concentrations (see the Methods section for details). For comparison, gas-sensing measurements performed on MWNTs functionalized with oxygen plasma ($O_2$-MWNTs sensors) are also reported. The morphology of the active layers and their chemical composition are characterized (Figure 1) using scanning electron microscopy (SEM), transmission electron microscopy (TEM), and X-ray photoelectron spectroscopy (XPS). The SEM image presents a thin mat of carbon nanotubes bridging the electrode gap (Figure 1a). The homogeneous dispersion of gold nanoparticles (average diameter ~10 nm) on the CNT sidewalls is illustrated in Figure 1b. The XPS spectrum (Figure 1c) of a typical sensor confirms the presence of Au on the MWNT network. Oxygen is also present due to the oxygen plasma functionalization of the CNTs, and the Si peaks are due to the substrate.

At room temperature, three different active layers ($O_2$-MWNTs, Au(5 Å)-MWNTs, and Au(10 Å)-MWNTs) are exposed to various concentrations of carbon monoxide, nitrogen dioxide, and benzene. Two sensors for each material were fabricated and studied, and each measurement was replicated three times. The responses

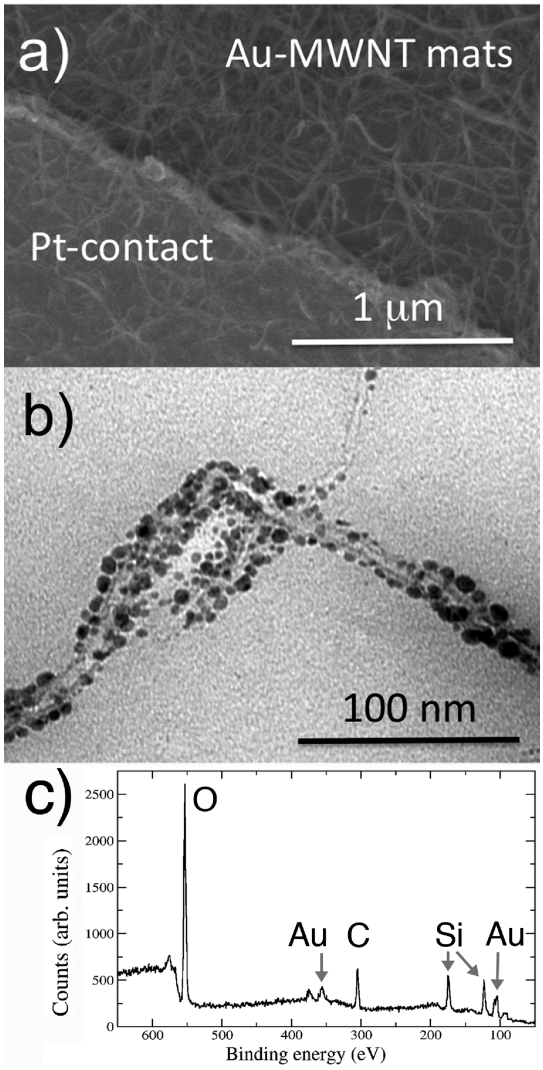


**Figure 1. Scanning (a) and transmission (b) electron microscopy images and X-ray photoelectron spectroscopy (c) of Au-MWNT sample.**

of the sensors to $NO_2$ and CO are displayed in Figure 2 and Figure 3. Figure 2 shows the change in sensor resistance *versus* time for increasing concentrations of $NO_2$. Figure 3, instead, illustrates the absolute response to CO (Figure 3a) and $NO_2$ (Figure 3b) of the different sensors. Figure 2a and Figure 2c are more affected by noise since the resistance of the MWNT mats is close to the lower measurement limit of the digital multimeter used for acquiring sensor resistance. The complete response of the sensors to $NO_2$ is reported in the Supporting Information, Figure S1 and S2. Both Au-MWNT and $O_2$-MWNT sensors are found to detect $NO_2$ down to 0.1 ppm and CO down to 2 ppm. However, Au-decorated MWNTs do improve the detection of both gases with respect to oxygen-functionalized MWNT sensors. The best response to $NO_2$ is achieved for Au(5 Å)-MWNT sensors (Figure 3b), because adsorption of $NO_2$ can occur both *via* the Au-NP and *via* the bare oxygenated-defected sites. Au decoration is, instead,

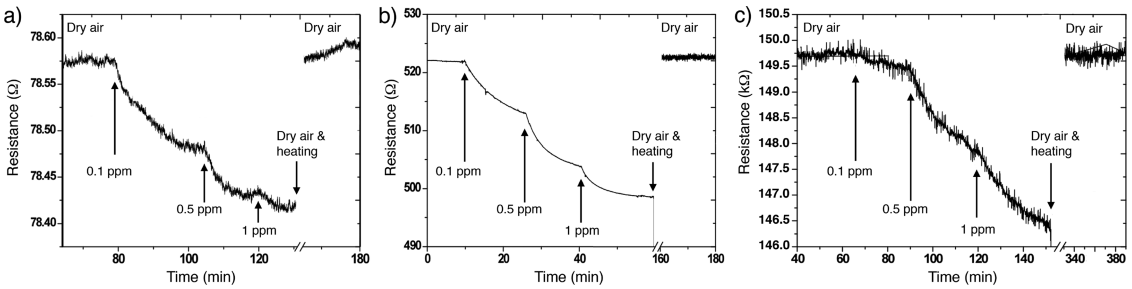


**Figure 2. Room-temperature response of the $O_2$-MWNT (a), Au(5 Å)-MWNT (b), and Au(10 Å)-MWNT (c) sensors toward $NO_2$.**

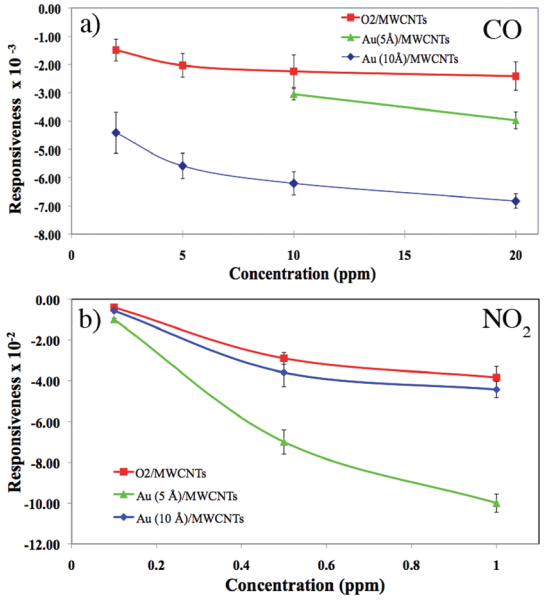


**Figure 3. Average responsiveness ($R$) of sensors based on $O_2$-MWNTs, Au(5 Å)-MWNTs, and Au(10 Å)-MWNTs for detection of CO (a) and $NO_2$ (b) at room temperature. The responsiveness is defined as $R = (R_g - R_a)/R_a$, where $R_g$ and $R_a$ are the values of resistance measured in the presence of gas and clean air, respectively.**

essential to improve CO detection (Figure 3a), since CO does not bind to oxygenated-defected sites.[30] This latter feature shows that the sensitivity of the sensors can be tuned by the synthesis conditions. All three kinds of sensors were also exposed to 1, 5, 7, and 10 ppm of benzene, but none of the tested sensors were able to detect this specific molecule.

**Structural and Electronic Properties.** MWNTs can be either metallic or semiconducting depending on the chirality of the individual shells and on the intershell interaction. A detailed description of their conductance is quite complex, but the main contribution to charge conduction around the Fermi energy is given by the outermost shell. Hence a SWNT can be used to approximately model the conductance of a MWNT.[2,31] Mats of MWNTs, such as those employed in the present experiment, consist of a mixture of metallic and semiconducting tubes. The conductance of the mat can be described as a percolation process through the contact points of metallic nanotubes, since a semiconducting tube would not allow electron conductance around the Fermi energy. Hence, a change in resistance of the mat would depend only on the metallic tubes. The tube diameter should not play a crucial role since the sensing mechanism is based on the catalytic properties of the metal NP rather than on the tube curvature. Finally, since the MWNT network consists of highly defective nanotubes, its resistance is mostly influenced by the resistance of individual nanotubes and not by internanotube or electrode−nanotube junctions.[32]

For these reasons, a (5,5) single-walled carbon nanotube (SWNT) decorated with a $Au_{13}$ nanoparticle in the presence of various gas molecules ($NO_2$, CO, $C_6H_6$) has been chosen as a model system. Using first-principles computational techniques (detailed in the Methods section), the NP-SWNT atomic structure has been optimized until the maximum force on each atom is less than 0.01 eV/Å and the maximum stress along the z direction of the unit cell (the transport direction) is smaller than 0.01 eV/Å. A 13-atom gold cluster has been chosen because $Au_{13}$ is close to the smallest cluster size for which the most stable structure is three-dimensional.[33] The decorations of a (5,5) SWNTs with $Au_{13}$ nanoclusters having initially cuboctahedral and icosahedral symmetries have both been considered. Even though the total energy of cuboctahedral $Au_{13}$ is ~1 eV lower than the icosahedral, the relaxed SWNT-icosahedral system has a total energy 1.15 eV lower and binding energy 0.6 eV higher than the relaxed SWNT-cuboctahedral. Hence, in the following discussion only (5,5) SWNTs decorated with icosahedral $Au_{13}$ NP are considered. After relaxation, the atomic structure of the adsorbed gold NP is quite distorted and the original symmetry of $Au_{13}$ is lost, as shown in Figure 4a. The Au NP binds weakly to the SWNT (Table 1) since the electronic d shell of gold is closed and, hence, the Au−C bond is not favored.[34] Consequently, the adsorption of $Au_{13}$ slightly perturbs the band structure of the SWNT (not shown here) and causes only a small shift of the Fermi energy toward lower energies, as schematically represented in Figure 5. This is equivalent to a p-doping of the tube, consistent with the small electronic charge transfer (~0.06 $e^-$) from the tube to the Au-NP.

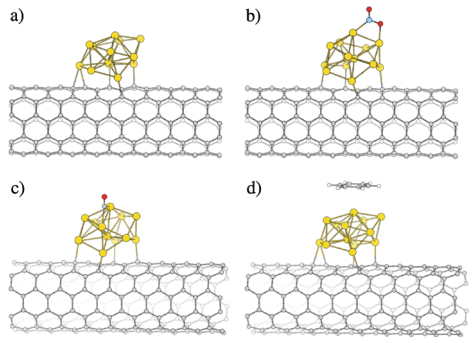


**Figure 4. Ball-and-stick models illustrating fully *ab initio* optimized atomic structures of a (5,5) SWNT decorated with a $Au_{13}$ nanocluster (a) and with various adsorbed molecules: $NO_2$ (b), CO (c), and $C_6H_6$ (d).**

**TABLE 1. Computed Binding Energies ($E_B$, eV), Charge Transfer ($\Delta q$, $|e|$), $Au_{13}$—SWNT Bond Length ($d_{Au}$, Å), and Molecule—$Au_{13}$ Bond Length ($d_{gas}$, Å)**

| | $Au_{13}$ | $NO_2$ | CO | $C_6H_6$ |
|---|---|---|---|---|
| $E_B$ | −2.444 | −3.257 | −1.821 | −0.193 |
| $d_{Au}$ | 2.38 | 2.39 | 2.35 | 2.38 |
| $d_{gas}$ | | 2.13 | 2.10 | 3.88 |
| $\Delta q^a$ | 0.06 | 0.506 | 0.164 | ∼0.0 |

[a] Positive (negative) values of $\Delta q$ denote an acceptor (donor) character of the corresponding adsorbed molecule.

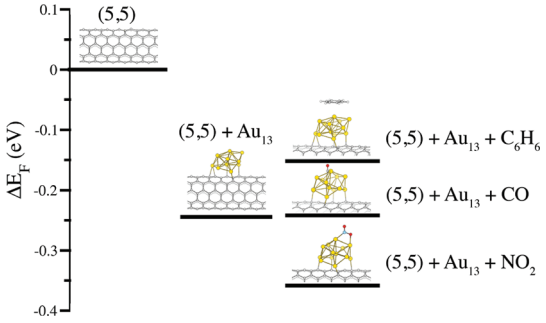


**Figure 5. Computed shift of the Fermi energy ($\Delta E_F$) of a pristine (5,5) SWNT after $Au_{13}$ decoration and after interaction with $C_6H_6$, CO, and $NO_2$ gas molecules.**

In order to model gas adsorption, first-principles conjugate gradient (CG) minimization is performed starting from molecules approaching the relaxed SWNT-NP system from several different initial configurations. The resulting ground-state geometries of $Au_{13}$-SWNT with and without adsorbed molecules are depicted in Figure 4. For each relaxed geometry, the computed bond lengths, binding energies, and charge transfer are collected in Table 1. Considerations based on basic chemistry/physics indicate that the relaxed structures can be considered as reliable. For instance, $NO_2$ is a polar molecule with positive charge localized on the nitrogen and negative charge on one of the oxygen atoms. Electron interaction with the gold NP will repel the negatively charged oxygen and attract the positively charged nitrogen, as shown in Figure 4b. Due to the high electronegativity of oxygen, the CO molecule would preferentially bind to gold through the carbon atom (Figure 4c), as also found in other works on adsorption of CO on various Au nanoclusters.[35] Lastly, the benzene—Au-CNT relaxed structure (Figure 4d) can be explained by considering that benzene would preferentially bind thanks to the delocalized $\pi$ electron ring, *i.e.*, with the benzene ring parallel to a gold surface. Gas adsorption is found not to alter the Au-SWNT interaction, as indicated by the almost unchanged Au-SWNT bond lengths. Computed binding energies and bong lengths show that $NO_2$ is the most strongly interacting molecule, while benzene is the less interacting one. $NO_2$ is predicted to accept a significant fraction of electronic charge (∼0.5 $e^-$) from the Au-SWNT system, consistent with the quite well-known electron acceptor character of that molecule. Indeed, the LUMO of $NO_2$ is located below the Fermi energy of the $Au_{13}$-(5,5) system, hence allowing a large charge transfer toward the molecule. The electron charge acquired by $NO_2$ is provided by both the Au-NP (which donates 0.289 $e^-$) and the (5,5) tube (which donates 0.218 $e^-$). The nature of the charge transfer between $NO_2$ and Au-SWNT indicates that the adsorbed molecule injects majority carriers, *i.e.*, holes, in the metal-decorated SWNT, hence strengthening its p-type semiconducting behavior and lowering further the Fermi energy of the system (Figure 5). The predicted injection of holes after $NO_2$ adsorption explains the decrease of resistance as measured in the Au-MWNT samples (Figure 2).

Due to the weak bonding between gold and carbon, it follows that the interaction between benzene, which consists of six carbon and six hydrogen atoms, and Au-SWNT is extremely weak and results only in an increase of the Fermi energy (Figure 5). However, the p-type semiconducting behavior of the overall system is maintained. It is worth noting that the shift of the Fermi energy with respect to a reference structure (in the present case, the Au-SWNT) indicates only the donor (increase of $E_F$) or acceptor (decrease of $E_F$) nature of the molecule and does not provide information on the actual occurrence of the charge transfer. The latter depends on the interaction strength between the molecule and Au-SWNT, *i.e.*, binding energy and bond length. The benzene—Au-SWNT interaction possesses all the characteristics of a physisorbtion, as indicated by the relatively large bond length (∼3.9 Å) and a low binding energy (−0.193 eV). The interaction is so weak that no significant charge transfer could be computed, suggesting that Au-decorated CNTs are not suitable for $C_6H_6$ detection, consistent with the result of the present experiments on Au-MWNT sensors. Metals that exhibit a stronger interaction with carbon should be more suitable for benzene detection, since the sensing mechanism relies on the binding of the gas

molecule to the nanocluster.[21] However, since the DFT formalism does not accurately model weak long-range interactions such as van der Waals forces, the real interaction between benzene and Au-SWNT could be stronger than the one predicted within the present *ab initio* approach. The inaccuracy in modeling van der Waals interactions will affect less the description of the detection of $NO_2$ and CO since these molecules bind iono-covalently to the Au nanocluster.

The adsorption of a single CO molecule on Au-CNT results in a small fraction of electron charge (0.164 $e^-$) transferred toward CO, but no shift of the Fermi energy is detectable with respect to the Au-CNT system (Figure 5). However, the interaction between CO and Au nanoclusters is quite complex[35] since it depends strongly on the overlap of the $5\sigma$ and $2\pi^*$ orbitals of the CO with the d orbitals of the gold NP, resulting in a mechanism of electron donation/back-donation. Indeed, CO donates electrons from its $\sigma$ orbitals to the $d_\sigma$ orbitals of gold and the filled $d_\pi$ orbitals of Au donate electrons back into the empty $\pi$ orbitals of CO.

**Quantum Electron Transport.** In order to check the sensing ability of CNTs, quantum transport calculations are performed by modeling the gas−Au-SWNT structure *via* an open system, consisting of a central scattering region and left and right semi-infinite electrodes. The contact electrodes (leads) are chosen as semi-infinite pristine (5,5) nanotubes, while the scattering region consists of nine "core" cells (including the metal NP and the molecule) sandwiched by three lead-like cells, in order to ensure a good screening of the perturbed Hartree potential due to the gas−metal system, as illustrated in ref 30. Since the coupling between the scattering region and the electrodes is strong and no external potential is considered, the NEGF formalism is equivalent to the Landauer−Büttiker formulation of equilibrium transport.[36] Within such an approach, the quantum electron conductance $G(E)$ and the transmission function $T(E)$ at a given energy $E$ are related by $G(E) = T(E)G_0$, and $G_0 = 2e^2/h$ is the quantum of conductance. As a result, the ballistic conductance of an ideal system at energy $E$ is proportional to the number of conducting channels, that is, the number of bands at that energy. For instance, the band structure of pristine armchair SWNTs is characterized by two bands crossing at the Fermi energy ($E_F$), resulting in a conductance of $2G_0$ in the corresponding energy window (Figure 6, dashed lines). Any perturbation of the ideal SWNT structure, such as metal decoration and/or gas adsorption, introduces new scattering centers, thus affecting the conductance curve, as illustrated in Figure 6. Au-functionalization of SWNTs induces several dips in the conductance curve of the pristine (5,5) tube (Figure 6a), and, in particular, the conductance at the Fermi energy $G(E_F)$ drops to $1G_0$, indicating the complete suppression of one transmission channel.

The adsorption of a single $NO_2$ molecule at the surface of the Au-NP results in a different distribution of the $G(E)$ dips (Figure 6b), with a remarkable increase of the conductance at the Fermi energy [$G(E_F)$] from $1G_0$ to $1.92G_0$ (+92%). Such a predicted enhancement of the conductance is consistent with the decrease of the resistance measured on the Au-decorated MWNT mats in the presence of $NO_2$ gas, as already presented in Figure 2b and Figure 2c. In addition, this result indicates that gold functionalization of CNTs improves the detection of $NO_2$ with respect to oxygenated-defected SWNTs, where adsorption of $NO_2$ was predicted[30] to cause a small change of $G(E_F)$ (4.6%) and the integration of the conductance curve over a properly selected energy interval around $E_F$ was needed to reveal $NO_2$ adsorption. The benefits of Au decoration of CNTs for $NO_2$ detection are also observed experimentally (Figure 3b).

The CO adsorption is also found to affect the conductance of Au-SWNTs (Figure 6c), but not as strongly as $NO_2$. In particular, the percentage change of $G(E_F)$ after CO adsorption corresponds to an increase of ~10%, hence predicting a small decrease in the resistance, in good agreement with the present experimental results (Figure 3). However, the predicted responsiveness of Au-SWNT detectors is similar to oxygenated-defected SWNTs,[30] while the experimental measurements suggest that Au functionalization improves the detection of CO (Figure 3). Such a discrepancy between experiments and simulations could be explained by the multiple adsorption of CO molecules on the same Au-NP that could happen experimentally, while the adsorption of a single CO molecule has been modeled. Indeed, the adsorption of more CO molecules affects further the computed conductance,[27] hence resulting in a stronger effect on the measured resistance. It is worth noting that charge transfer considerations alone are not sufficient to describe the electrical behavior of CNTs, especially in the case of CO, whose interaction with gold is quite complex, as it involves a charge transfer in both directions: *to* and *from* the CO molecule. A more powerful tool such as NEGF quantum conductance calculations corroborated by a careful analysis of the $G(E)$ curve is thus mandatory to make accurate predictions.

Lastly, the adsorption of $C_6H_6$ leaves the overall shape of the conductance curve almost unaffected (Figure 6d). The percentage change of $G(E_F)$ is less than 5%, suggesting that it would be quite difficult to achieve benzene detection *via* a measurement of resistance in Au-decorated CNTs. This theoretical prediction is also consistent with the experiments. Indeed, neither the $O_2$-MWNT or Au-MWNT sensors were responsive to benzene for any tested concentration.

Finally, it should be noted that a quantitative description of realistic gas sensors should take into account the effect of configurational disorder. However,

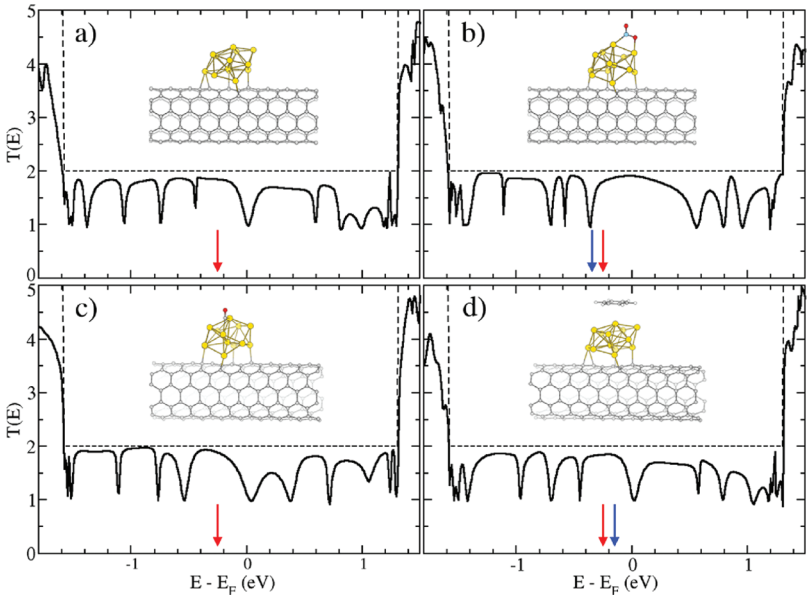


**Figure 6. Quantum conductance of a (5,5) SWNT decorated with a $Au_{13}$ nanocluster (a) and with various adsorbed molecules: $NO_2$ (b), CO (c), and $C_6H_6$ (d) at the surface of this gold cluster. The energy zero is aligned with the Fermi energy of a pristine (5,5) tube, the red arrow at −0.25 eV indicates the Fermi energy of the $Au_{13}$−(5,5) system, while the blue arrow in panels (b) and (d) indicates the Fermi energy in the presence of $NO_2$ (b) and $C_6H_6$ (d). The position of the Fermi level is unchanged after CO adsorption.**

the decrease (or increase) of conductance after gas adsorption will remain unchanged even when ~300 random distributions of such configuration are considered.[37] Hence, the study of individual configurations can reasonably be used to understand and analyze experimental results.

## CONCLUSIONS

In conclusion, the experimental measurements related to the detection of several gases ($NO_2$, CO, and $C_6H_6$) *via* mats of MWNTs functionalized with oxygen plasma and decorated with Au nanoparticles are corroborated by first-principles quantum electron conductance calculations performed on a $Au_{13}$-SWNT model. Both simulations and experiments predict that gold decoration of CNTs improves the detection of $NO_2$ and CO with respect to oxygenated-defected CNTs, while benzene remains undetected. In particular, in the case of $NO_2$ detection, the computed shift of the Fermi energy and the nature of the charge transfer are directly correlated to the resistance decrease measured experimentally, suggesting electronic mechanisms at the microscopic level that can be extrapolated at the macroscopic level to explain the Au-CNT behavior in the presence of specific gas molecules. However, charge transfer considerations alone are not sufficient to describe how carbon oxide adsorption affects the resistance of the Au-CNTs. Indeed, in the latter case, quantum electron transport simulations have proven to be essential to predict the decrease of the resistance, in agreement with the experimental data. Finally, the lack of benzene sensitivity is explained in terms of the weak interaction strength that arises between the molecule and the Au-NP, but also between that particle and the nanotube. It is worth noting that the present predictions should also be valid in water-wet situations, since the average conductance of CNTs has been shown to be almost unaffected by electrostatic disorder.[38] The present combined experimental/theoretical approach has been proved crucial to provide microscopic insight concerning the behavior of gas sensors based on metal-decorated CNTs. This research also illustrates how first-principles techniques can be used as powerful predictive tools to understand, improve, and design the next generation of gas sensors.

## METHODS: EXPERIMENT

On the experimental side, commercially available MWNTs from Nanocyl were used. The outer diameters of the tubes ranged from 3 to 15 nm, and their length was about 50 $\mu$m. Although SWNTs are known to be more sensitive to gas molecules than MWNTs, the latter are cheaper and more easily produced on a large scale. Therefore MWNTs are more suitable for the fabrication of inexpensive gas sensors. In order to promote Au adhesion, as-received MWNTs undergo an oxygen plasma treatment in a cold, low-pressure plasma reactor and are subsequently decorated with Au NPs using thermal evaporation, as reported in ref 39. The effect of the $O_2$ plasma on the CNT surface consists in breaking several C−C bonds, thus creating active sites where the Au atoms are trapped and cluster in

NPs.[17,26] The plasma pretreatment mostly influences the wetting of the CNT walls by the metal and has only a secondary influence on the sensitivity to chemical species. In ref 40 the treatment of CNT sidewalls with Ar and Ar plus $O_2$ plasma has been compared, revealing that the presence of oxygen in the plasma significantly increases the amount of metal nanoparticles attached to CNT sidewalls. Hence, for the present study, the $O_2$ plasma pretreatment has been employed. Two different amounts of Au are evaporated on the plasma-treated MWNTs, corresponding to 5 and 10 Å films coating the surface of a quartz crystal microbalance situated inside the thermal evaporation chamber. This procedure leads to MWNTs decorated with a significantly different amount of Au nanoparticles[39] denoted Au(5 Å)-MWNTs and Au(10 Å)-MWNTs. The Au-MWNTs are dispersed in dimethylformamide (DMF), and the obtained solution is drop coated onto platinum comb electrodes placed on silicon micromachined substrates that included an embedded heating resistor. The substrate is a stack of thin silicon nitride, polysilicon, and silicon oxide layers. Metal-decorated carbon nanotubes sit on top of the electrically insulating silicon dioxide layer, and, therefore, the substrate is not expected to play any active role in the charge transfer between adsorbed species and the Au-decorated CNTs. An in-depth description of the sensor substrate can be found in ref 41. Silicon substrates undergo a thermal treatment as described in refs 21 and 26 in order to impose complete removal of the organic vehicle and promote adhesion of MWNT mats to the substrate.

## METHODS: MODELING

Ground-state calculations are performed within the *ab initio* density functional theory (DFT) formalism,[42] and quantum electron transport is modeled within the nonequilibrium Green's function (NEGF) approach using the one-particle DFT Hamiltonian.[43] All the calculations are performed using norm-conserving pseudopotentials[44] and the local spin density approximation (LSDA). Indeed, while the $Au_{13}$-CNT system (with and without adsorbed molecules) is found not to be spin-polarized, the isolated $Au_{13}$ cluster is magnetic.[45] A numerical atomic orbital basis set of double-$\zeta$ quality is used for C and of double-$\zeta$ plus one polarization orbital for N, both with 272 meV energy shift. An optimized basis of quality double-$\zeta$ plus one polarization orbital is employed for Au, O, and H.[46] Periodic boundary conditions with fixed lateral dimensions are used to ensure ~18 Å of vacuum between the SWNTs in neighboring cells. Due to the presence of the metallic NP, a $1 \times 1 \times 9$ supercell is considered, leading to a distance between NPs of ~14.8 along the tube and a linear density of gas molecules of ~4.5%, *i.e.*, one adsorbed molecule every 22 Å. The real-space grid cutoff is 400 Ry, the k-point sampling mesh is $1 \times 1 \times 14$, and a Fermi−Dirac distribution function with an electronic temperature of 10 meV is used to populate the energy levels. Basis set quality, k-point sampling, kinetic energy cutoff, and electronic temperature have been chosen after accurate convergence studies on the structural, electronic, and quantum transport properties of the $Au_{13}$-SWNT model. Binding energies are corrected for the basis set superposition error (BSSE),[47] and atomic charges are obtained with the Bader decomposition analysis.[48,49] The technical details related to the computation of the transport properties are the same as for the ground-state calculations with the exception of the real-space grid cutoff, which has been raised to 600 Ry in order to guarantee a more accurate description of the electrostatic potential.

*Acknowledgment.* J.-C.C. acknowledges financial support from the F.R.S.-FNRS of Belgium. Parts of this work are directly connected to the Nano2Hybrids project (EC-STREP-033311), to the Belgian Program on Interuniversity Attraction Poles (PAI6) on "Quantum Effects in Clusters and Nanowires", to the ARC on "Hybrid metal/organic nanosystems" sponsored by the Communauté Française de Belgique, and to the European Union through the ETSF e-I3 project (Grant No. 211956). Computational resources have been provided by the supercomputing facilities of the Université Catholique de Louvain (CISM). E.L. acknowledges financial support from the Catalan Government under Grant No. 2009 SGR 789.

*Supporting Information Available:* Additional experimental results. This material is available free of charge *via* the Internet at http://pubs.acs.org.

## REFERENCES AND NOTES

1. Iijima, S. Helical Microtubules of Graphitic Carbon. *Nature* **1991**, *354*, 56–58.
2. Charlier, J.-C.; Blase, X.; Roche, S. Electronic and Transport Properties of Nanotubes. *Rev. Mod. Phys.* **2007**, *79*, 677–732.
3. Dubois, S. M. M.; Zanolli, Z.; Declerck, X.; Charlier, J. C. Electronic Properties and Quantum Transport in Graphene-Based Nanostructures. *Eur. Phys. J. B* **2009**, *72*, 1–24.
4. Avouris, P.; Chen, Z.; Perebeinos, V. Carbon-Based Electronics. *Nat. Nanotechnol.* **2007**, *2*, 605–615.
5. Tsukagoshi, K.; Alphenaar, B.; Ago, H. Coherent Transport of Electron Spin in a Ferromagnetically Contacted Carbon Nanotube. *Nature* **1999**, *401*, 572–574.
6. Sahoo, S.; Kontos, T.; Furer, J.; Hoffmann, C.; Graber, M.; Cottet, A.; Schonenberger, C. Electric Field Control of Spin Transport. *Nat. Phys.* **2005**, *1*, 99–102.
7. Hueso, L. E.; Pruneda, J. M.; Ferrari, V.; Burnell, G.; Valdes-Herrera, J. P.; Simons, B. D.; Littlewood, P. B.; Artacho, E.; Fert, A.; Mathur, N. D. Transformation of Spin Information into Large Electrical Signals using Carbon Nanotubes. *Nature* **2007**, *445*, 410–413.
8. Hauptmann, J. R.; Paaske, J.; Lindelof, P. E. Electric-Field-Controlled Spin Reversal in a Quantum Dot with Ferromagnetic Contacts. *Nat. Phys.* **2008**, *4*, 373–376.
9. Bianco, A.; Kostarelos, K.; Prato, M. Applications of Carbon Nanotubes in Drug Delivery. *Curr. Opin. Chem. Biol.* **2005**, *9*, 674–679.
10. Lu, F.; Gu, L.; Meziani, M. J.; Wang, X.; Luo, P. G.; Veca, L. M.; Cao, L.; Sun, Y.-P. Advances in Bioapplications of Carbon Nanotubes. *Adv. Mater.* **2009**, *21*, 139–152.
11. Liu, Z.; Tabakman, S. M.; Chen, Z.; Dai, H. Preparation of Carbon Nanotube Bioconjugates for Biomedical Applications. *Nat. Protoc.* **2009**, *4*, 1372–1382.
12. Goldoni, A.; Petaccia, L.; Lizzit, S.; Larciprete, R. Sensing Gases with Carbon Nanotubes: a Review of the Actual Situation. *J. Phys. Condens. Matter* **2010**, *22*, 013001.
13. Peng, S.; Cho, K. Ab Initio Study of Doped Carbon Nanotube Sensors. *Nano Lett.* **2003**, *3*, 513–517.
14. *Metal Nanoparticles: Synthesis, Characterization and Applications*; Foss, C. J., Feldheim, D., Eds.; Marcel Dekker: New York, 2002.
15. Kong, J.; Chapline, M.; Dai, H. Functionalized Carbon Nanotubes for Molecular Hydrogen Sensors. *Adv. Mater.* **2001**, *13*, 1384–1386.
16. Star, A.; Joshi, V.; Skarupo, S.; Thomas, D.; Gabriel, J.-C. P. Gas Sensor Array Based on Metal-Decorated Carbon Nanotubes. *J. Phys. Chem. B* **2006**, *110*, 21014–21020.
17. Bittencourt, C.; Felten, A.; Espinosa, E.; Ionescu, R.; Llobet, E.; Corteig, X.; Pireaux, J. $WO_3$ Films Modified with Functionalised Multi-Wall Carbon Nanotubes: Morphological, Compositional and Gas Response Studies. *Sens. Actuators, B* **2006**, *115*, 33–41.
18. Espinosa, E. H.; Ionescu, R.; Bittencourt, C.; Felten, A.; Erni, R.; Van Tendeloo, G.; Pireaux, J.-J.; Llobet, E. Metal-Decorated Multi-Wall Carbon Nanotubes for Low Temperature Gas Sensing. *Thin Solid Films* **2007**, *515*, 8322–8327.

19. Kauffman, D. R.; Star, A. Chemically Induced Potential Barriers at the Carbon Nanotube-Metal Nanoparticle Interface. *Nano Lett.* **2007**, *7*, 1863–1868.
20. Penza, M.; Rossi, R.; Alvisi, M.; Cassano, G.; Signore, M. A.; Serra, E.; Giorgi, R. Pt- and Pd-Nanoclusters Functionalized Carbon Nanotubes Networked Films for sub-ppm Gas Sensors. *Sens. Actuators, B* **2008**, *135*, 289–297.
21. Leghrib, R.; Felten, A.; Demoisson, F.; Reniers, F.; Pireaux, J.-J.; Llobet, E. Room-Temperature, Selective Detection of Benzene at Trace Levels using Plasma-Treated Metal-Decorated Multiwalled Carbon Nanotubes. *Carbon* **2010**, *48*, 3477–3484.
22. Khalap, V. R.; Sheps, T.; Kane, A. A.; Collins, P. G. Hydrogen Sensing and Sensitivity of Palladium-Decorated Single-Walled Carbon Nanotubes with Defects. *Nano Lett.* **2010**, *10*, 896–901.
23. Zhao, Q.; Nardelli, M.; Lu, W.; Bernholc, J. Carbon Nanotube-Metal Cluster Composites: A New Road to Chemical Sensors? *Nano Lett.* **2005**, *5*, 847–851.
24. Pannopard, P.; Khongpracha, P.; Probst, M.; Limtrakul, J. Gas Sensing Properties of Platinum Derivatives of Single-Walled Carbon Nanotubes: a DFT Analysis. *J. Mol. Graphics Modell.* **2009**, *28*, 62–69.
25. Wang, R.; Zhang, D.; Sun, W.; Han, Z.; Liu, C. A Novel Aluminum-Doped Carbon Nanotubes Sensor for Carbon Monoxide. *J. Mol. Struct. (THEOCHEM)* **2007**, *806*, 93–97.
26. Charlier, J.-C.*et al*. Carbon Nanotubes Randomly Decorated with Gold Clusters: from Nano(2)Hybrid Atomic Structures to Gas Sensing Prototypes. *Nanotechnology* **2009**, *20*, 375501.
27. Kauffman, D. R.; Sorescu, D. C.; Schofield, D. P.; Allen, B. L.; Jordan, K. D.; Star, A. Understanding the Sensor Response of Metal-Decorated Carbon Nanotubes. *Nano Lett.* **2010**, *10*, 958–963.
28. Pengfei, Q.; Vermesh, O.; Grecu, M.; Javey, A.; Wang, O.; Dai, H.; Peng, S.; Cho, K. Toward Large Arrays of Multiplex Functionalized Carbon Nanotube Sensors for Highly Sensitive and Selective Molecular Detection. *Nano Lett.* **2003**, *3*, 347–351.
29. Zhang, Y.; Franklin, N.; Chen, R.; Dai, H. Metal Coating on Suspended Carbon Nanotubes and its Implication to Metal-Tube Interaction. *Chem. Phys. Lett.* **2000**, *331*, 35–41.
30. Zanolli, Z.; Charlier, J. C. Defective Carbon Nanotubes for Single-Molecule Sensing. *Phys. Rev. B* **2009**, *80*, 155447.
31. Forro, L.; Schonenberger, C. Physical Properties of Multi-Wall Nanotubes. In *Carbon Nanotubes*; Springer-Verlag Berlin: Berlin, Germany, 2001; Vol. 80, pp 329−390.
32. Salehi-Khojin, A.; Khalili-Araghi, F.; Kuroda, M. A.; Lin, K. Y.; Leburton, J.-P.; Masel, R. I. On the Sensing Mechanism in Carbon Nanotube Chemiresistors. *ACS Nano* **2010**, *5*, 153–158.
33. Gruber, M.; Heimel, G.; Romaner, L.; Bredas, J.-L.; Zojer, E. First-Principles Study of the Geometric and Electronic Structure of Au-13 Clusters: Importance of the Prism Motif. *Phys. Rev. B* **2008**, *77*, 165411.
34. Park, N.; Sung, D.; Lim, S.; Moon, S.; Hong, S. Realistic Adsorption Geometries and Binding Affinities of Metal Nanoparticles onto the Surface of Carbon Nanotubes. *Appl. Phys. Lett.* **2009**, *94*, 073105.
35. Mpourmpakis, G.; Andriotis, A. N.; Vlachos, D. G. Identification of Descriptors for the CO Interaction with Metal Nanoparticles. *Nano Lett.* **2010**, *10*, 1041–1045.
36. Buttiker, M.; Imry, Y.; Landauer, R.; Pinhas, S. Generalized Many-Channel Conductance Formula with Application to Small Rings. *Phys. Rev. B* **1985**, *31*, 6207–6215.
37. Rocha, A. R.; Rossi, M.; Fazzio, A.; da Silva, A. J. R. Designing Real Nanotube-Based Gas Sensors. *Phys. Rev. Lett.* **2008**, *100*, 176803.
38. Rungger, I.; Chen, X.; Schwingenschloegl, U.; Sanvito, S. Finite-Bias Electronic Transport of Molecules in a Water Solution. *Phys. Rev. B* **2010**, *81*, 235407.
39. Bittencourt, C.; Felten, A.; Douhard, B.; Colomer, J.-F.; Van Tendeloo, G.; Drube, W.; Ghijsen, J.; Pireaux, J.-J. Metallic Nanoparticles on Plasma Treated Carbon Nanotubes: Nano(2)hybrids. *Surf. Sci.* **2007**, *601*, 2800–2804.
40. Claessens, N.; Demoisson, F.; Dufour, T.; Mansour, A.; Felten, A.; Guillot, J.; Pireaux, J.-J.; Reniers, F. Carbon Nanotubes Decorated with Gold, Platinum and Rhodium Clusters by Injection of Colloidal Solutions into the Post-Discharge of an RF Atmospheric Plasma. *Nanotechnology* **2010**, *21*, 385603–385609.
41. Ionescu, R.; Espinosa, E.; Sotter, E.; Llobet, E.; Vilanova, X.; Correig, X.; Felten, A.; Bittencourt, C.; Van Lier, G.; Charlier, J.; Pireaux, J. Oxygen Functionalisation of MWNT and their use as Gas Sensitive Thick-Film Layers. *Sens. Actuators, B* **2006**, *113*, 36–46.
42. Soler, J. M.; Artacho, E.; Gale, J. D.; Garcia, A.; Junquera, J.; Ordejon, P.; Sanchez-Portal, D. The SIESTA Method for Ab Initio Order-N Materials Simulation. *J. Phys.: Condens. Matter* **2002**, *14*, 2745–2779.
43. Rocha, A. R.; Garcia-Suarez, V. M.; Bailey, S.; Lambert, C.; Ferrer, J.; Sanvito, S. Spin and Molecular Electronics in Atomically Generated Orbital Landscapes. *Phys. Rev. B* **2006**, *73*, 085414.
44. Troullier, N.; Martins, J. L. Efficient Pseudopotentials for Plane-Wave Calculations. *Phys. Rev. B* **1991**, *43*, 1993–2006.
45. Yamamoto, Y.; Hori, H. Direct Observation of the Ferromagnetic Spin Polarization in Gold Nanoparticles: A Review. *Rev. Adv. Mater. Sci.* **2006**, *12*, 23–32.
46. Junquera, J.; Paz, O.; Sanchez-Portal, D.; Artacho, E. Numerical Atomic Orbitals for Linear-Scaling Calculations. *Phys. Rev. B* **2001**, *64*, 235111.
47. Boys, S.; Bernardi, F. Calculation of Small Molecular Interactions by Differences of Separate Total Energies - Some Procedures with Reduced Errors. *Mol. Phys.* 1970, *19*, 553.
48. Bader, R. F. W. *Atoms in Molecules - A Quantum Theory*; Oxford University Press: Oxford, 1990.
49. Sanville, E.; Kenny, S. D.; Smith, R.; Henkelman, G. Improved Grid-Based Algorithm for Bader Charge Allocation. *J. Comput. Chem.* **2007**, *28*, 899–908.